4. Pipe-arches are easy to place using normal construction equipment. Arch structures require more sophisticated handling equipment and techniques because of their size, shape, and weight.

5. Pipe-arches have only experienced some scour and sedimentation problems. Arch structures are relatively new and somewhat experimental in nature, but to date they have not directly presented similar maintenance or repair problems.

6. It appears that up to two lines of pipe-arches are as economical to use as a single arch structure. However, three or more lines of pipe-arches are significantly more expensive than a single arch structure.

Publication of this paper sponsored by Committee on Culverts and Hydraulic Structures.

Measurements and Analyses of Compaction Effects on a Long-Span Culvert

RAYMOND B. SEED AND CHANG-YU OU

Earth pressures that result from compaction of backfill can induce stresses and deformations, which are not amenable to analysis by conventional analytical methods, in flexible metal culverts. In this paper are presented the results of a study in which deformations of a 39-ft-span flexible metal culvert were measured at various stages of backfill placement and compaction. These field measurements were then compared with the results of finite element analyses in order to investigate the influence of compaction effects on culvert stresses and deformations. Two types of finite element analyses were performed: *(a)* conventional analyses that make no provision for modeling compaction effects and *(b)* analyses that incorporate recently developed models and analytical procedures that permit modeling of compaction-induced stresses and deformations. The results of these finite element analyses indicate that compaction effects significantly increased structural deformations during backfilling and also significantly affected bending moments within the culvert. Axial thrust around the culvert perimeter was also affected by compaction-induced earth pressures, but to a lesser degree. The results of this study provide a basis for assessing the potential importance of considering compaction effects in evaluating culvert stresses and deformations during and after backfill placement and compaction.

Earth pressures that result from compaction of backfill can produce stresses and deformations, which are not amenable to analysis by conventional analytical methods, in flexible metal culverts. These compaction-induced stresses and deformations can significantly influence the stress state and geometry of a culvert at various stages of backfill placement and compaction.

In this paper are presented the results of a study in which deformations of a large-span flexible metal culvert structure were measured during backfill operations. Detailed records of backfill placement procedures were maintained and care was taken to prevent the operation of large construction equipment in close proximity to the culvert, so this field study represents a case in which the influence of compaction effects on culvert stresses and deformations was less pronounced than for more typical cases in which the proximity of large equipment to the culvert structure is less rigorously controlled.

Two types of finite element analyses were performed: (*a*) conventional analyses that are well able to model incremental placement of backfill in layers but that cannot model compaction-induced stresses and deformations and (*b*) analyses that incorporate recently developed models and analytical procedures that permit modeling of compaction effects (*1*, *2*). Comparison of the results of these two types of analyses with each other, as well as with field measurements, provides a basis for assessing the potential importance of considering compaction effects in analyzing culvert stresses and deformations.

PROMONTORY CULVERT STRUCTURE

The Promontory culvert structure is located in Mesa, California, and is designed to perform as a bridge providing grade separation between two otherwise intersecting roadways. Figure 1 (top) shows a cross section through the structure. The culvert is a low-profile arch, with a span of 38 ft 5 in., a rise of 15 ft 9 in., and a length of 80 ft, founded on 3-ft-high reinforced concrete stem walls with a reinforced concrete base slab. The culvert consists of 9- x 2 1/2-in. corrugated aluminum structural plate 0.175 in. thick, and the crown section is reinforced with Type IV aluminum bulb angle stiffener ribs that occur at a spacing of 9 in. The culvert haunches are grouted into a slot at the top of the stem walls, providing a rigid connection for moment transfer at this point.

The existing foundation soil at the site was a stiff, silty, sandy clay of low plasticity (CL-SC). Chemical tests indicated that this sandy clay was potentially corrosive with respect to the culvert structure. As a result, a crushed basalt material (select fill) was imported for use as a protective backfill envelope within 3 to 4 ft of the culvert. This crushed basalt was an angular silty sand (SM) and was placed to a minimum width of 4 ft at both sides of the culvert and continued to the final fill surface as shown in Figure 1 (top).

Department of Civil Engineering, Stanford University, Stanford, Calif. 94305.

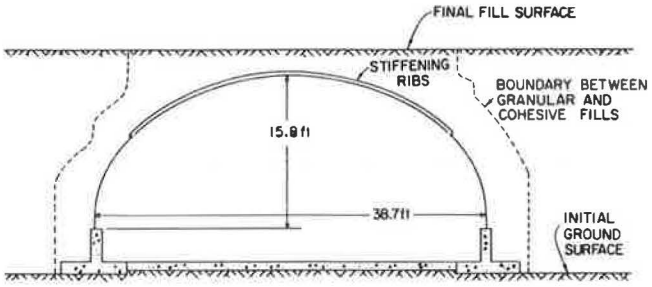

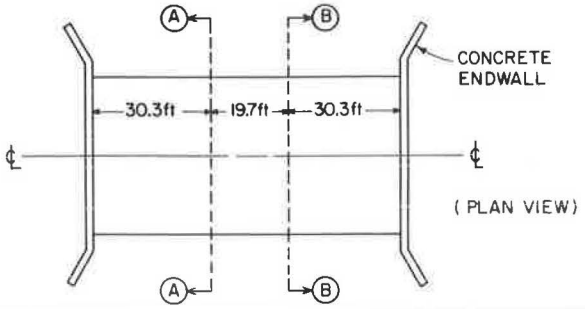

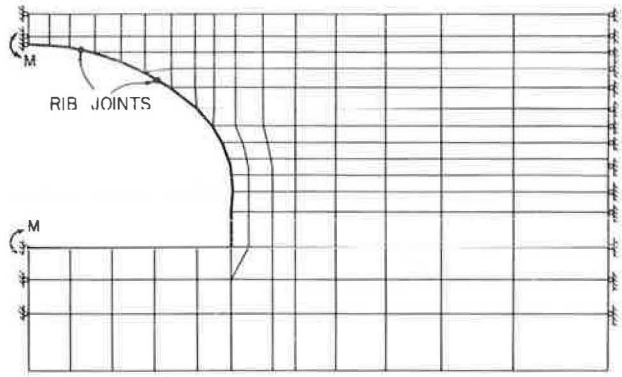

FIGURE 1 Promontory overpass structure.

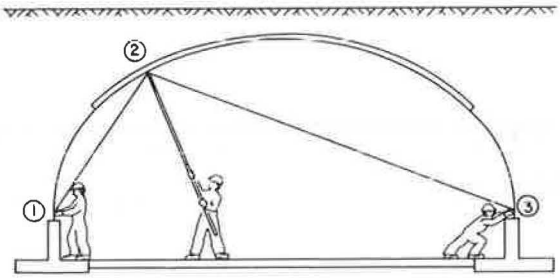

FIGURE 2 Measurements of culvert deformations during backfilling.

The existing sandy clay was used as backfill outside of this select fill zone. Both materials were compacted to a minimum of 95 percent of the maximum dry density determined by a standard Proctor compaction test (ASTM 698–D). Backfill placement and compaction procedures will be discussed later in detail. The final depth of soil cover over the crown of the structure was 2.5 ft.

FIELD MEASUREMENTS OF DEFORMATIONS DURING BACKFILLING

Culvert deformations were monitored at two culvert sections during backfill placement and compaction. As shown in Figure 2 (top), these sections (A-A and B-B) were separated by 19.7 ft and were both located 30.3 ft from the ends of the culvert to avoid any influence of restraint provided by the two reinforced concrete end walls. At both cross sections, the displacements of 13 measurement points were monitored relative to a pair of reference points at the base of the culvert haunches, as shown in Figure 2 (bottom). The change in span between the two reference points was also measured, and all relative displacements were corrected accordingly. Monitoring the relative displacements of these 15 points permitted determination of the deformed shape of each of the full cross sections at any given stage of backfill operations.

The distances between the measuring points and each of the two reference points at each section were measured using lightweight steel tapes. The measuring points were permanently established by means of marker bolts, and the ends of the steel tapes were held to the ends of these bolts by means of a fixture at the end of a pole that was designed to mate consistently with the measuring points. Tape tension was kept constant, and no correction was made for thermal expansion or contraction of the tape because the estimated maximum correction was less than 1/16 in. under the least favorable conditions encountered. Numerous practice measurements were taken before backfill operations began until it was demonstrated that all measurements could be repeated consistently within ± 3/32 in., with readings taken to the nearest 1/32 in. At the end of each day of construction operations a number of the most recent measurements were repeated at random to verify that this level of accuracy was maintained.

Backfill operations were well controlled and measured deformations at Sections A-A and B-B were nearly identical at all backfill stages, as shown in Figure 3, which shows the final deformed culvert shapes at both measured sections on completion of backfill placement and compaction. In this figure, deformations are exaggerated by a scaling factor of 5 for clarity. Throughout the remainder of this paper, all "measured" deformations reported will represent averaged deformations for the two measured sections.

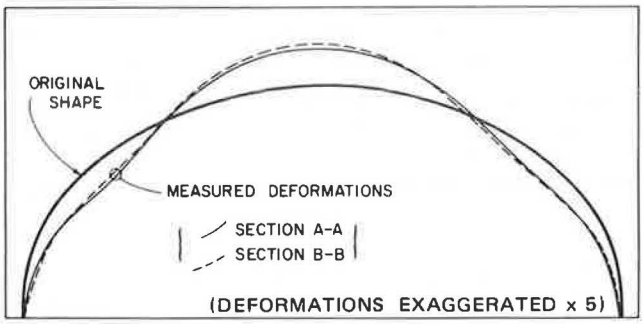

FIGURE 3 Final deformed shapes of Measurement Sections A-A and B-B.

Figure 4 shows measured deformations at three backfill stages: (*a*) backfill midway up the haunches, (*b*) backfill approximately 1.5 ft below the crown, and (*c*) final soil cover depth of 2.5 ft. Deformations are again exaggerated by a factor of 5. The general

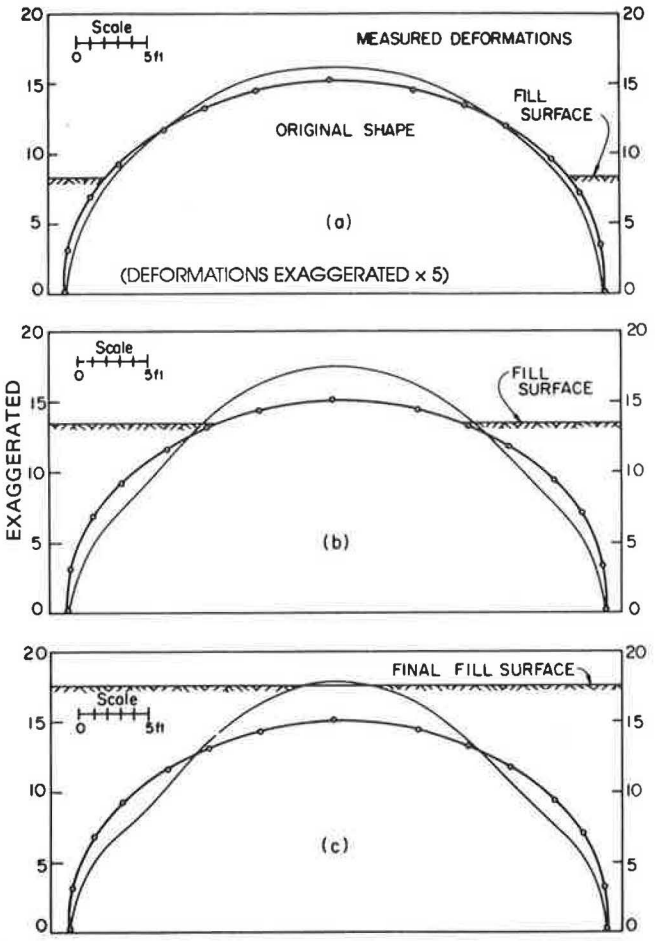

FIGURE 4 Measured deformations at various backfill stages.

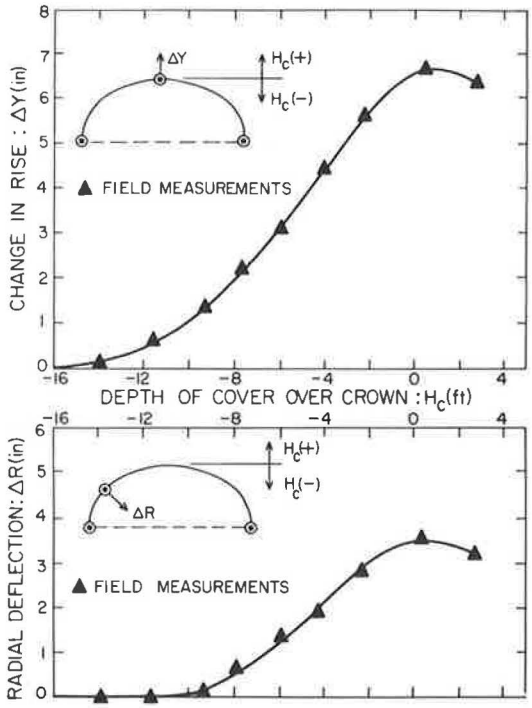

FIGURE 5 Measured crown rise and radial quarter point deflection versus fill height.

pattern of culvert deformations consisted of decreasing span and inward flexure of the quarter points at the juncture of the haunch and crown sections with increasing fill height, accompanied by an upward movement of the crown ("peaking"). The backfill elevation was carefully maintained at nearly the same level on both sides of the culvert at all fill stages, and placement and compaction operations were nearly identical on both sides of the culvert at any given fill stage, which resulted in essentially symmetric deformations of both sides of the culvert as shown in Figure 4. Maximum peaking of the crowns of both measured culvert sections were approximately 6.6 in., and the maximum inward radial deflection at the upper haunches was approximately 3.6 in.

The measured culvert deformations can be well characterized by monitoring the vertical deflection of the crown point and the radial deformation of the quarter point, as shown in Figures 4 and 5. In Figure 5, which shows crown and quarter point deflections as a function of backfill level, it can be seen that, as backfill was placed above the crown of the structure, peaking reversed and the crown began to descend slightly under the weight of the new crown cover fill.

FIELD OBSERVATIONS DURING BACKFILL OPERATIONS

Several important factors that affect the magnitude of compaction-induced soil stresses at any given point in the ground are contact pressure, footprint geometry, and closest proximity to the point of interest achieved by any given compaction (or other construction) vehicle. This is because these factors control the peak stress increase induced at the point of interest during application of the transient surface load represented by the most critical positioning of the compaction vehicle, and residual compaction-induced stresses remaining after departure of this transient vehicle load are a direct function of this peak stress increase (*1*).

During backfill placement and compaction, large equipment and vehicles were not allowed to operate in close proximity to the culvert structure. As a result, compaction-induced earth pressures acting against the culvert were quite sensitive to the closest proximity to the culvert achieved by each piece of compaction equipment at each backfill stage. To properly model compaction-induced earth pressures acting against the culvert, it was thus necessary to continuously monitor the closest proximity to the culvert achieved by each construction vehicle at each stage of backfill placement and compaction, and field observers maintained a detailed record of this.

Six types of construction equipment were used during backfill operations: (*a*) a small pan or scraper, (*b*) a tracked bulldozer, (*c*) a front loader with four rubber wheels, (*d*) a 2,000-gal water truck, (*e*) a two-drum vibratory hand roller, and (*f*) a medium-sized single-drum vibratory roller. Table 1 gives the significant characteristics of each of these pieces of equipment that affect the magnitude of compaction-induced soil stresses within the backfill.

Backfill operations began with the initial ground surface at the base of the concrete stem walls. Up to an elevation of 10 ft above the stem wall bases (near the top of the culvert haunches) the select backfill envelope was maintained at a width of from 4 to 4.5 ft and was placed and compacted in 6-in. lifts. The select fill was dumped by the front loader operating at some distance from the culvert and was spread by hand before being compacted by the two-drum vibratory hand roller, so that the hand roller was the only equipment operated close to the culvert. The native backfill was brought

TABLE 1 EQUIPMENT USED FOR BACKFILL PLACEMENT AND COMPACTION

Attribute	Measurement
John Deere JD-672 scraper	
Wheel type	4 rubber tires
Lateral tire separation	7.5 ft (center to center)
Axle spacing	26 ft
Operating weight modeled	62 kips (60% on rear axle)
Caterpiller CAT D6D dozer	
Tread spacing	74 in. (center to center)
Tread contact length	93 in.
Operating weight modeled	32 kips
Case W20-C front loader	
Wheel type	4 rubber tires
Lateral tire separation	73 in.
Axle spacing	108 in.
Operating weight modeled	23 kips (60% on front axle)
2,000-gal water truck	
Front axle	2 rubber tires at 6.5 ft
Rear axle	4 rubber tires (total width = 8.5 ft)
Axle spacing	10 ft
Operating weight modeled	47 kips
Wacker WDH 86-110(758) two-drum vibratory roller	
Drum length	32 in.
Drum spacing	40 in. (center to center)
Total weight	2.8 kips
Peak dynamic thrust	Modeled at 6.3 kips/drum
Raygo SF-54A single-drum vibratory roller	
Drum length	54 in.
Total weight	4.8 kips
Peak dynamic thrust	15 kips

up roughly concurrently with the select fill envelope and was rolled right to the point of contact with the select fill by both the water truck and the scraper, so that both of these heavy vehicles operated over the full fill surface to within a proximity of approximately 4 to 4.5 ft to the culvert haunches.

As the fill began to rise above the haunches and onto the ribbed crown section, the select fill envelope began to follow the culvert contour, as shown in Figure 1 (top). Until the fill reached an elevation approximately 1 ft below the crown, the select fill continued to be hand leveled and compacted with the hand roller, though the bulldozer began to operate on the outer edges of the select zone. The native soil lifts at this stage were again rolled by the scraper and water truck, and both vehicles made occasional (documented) incursions onto the select fill zone.

At a fill elevation approximately 1 ft below the crown, the larger single-drum vibratory roller (towed by the bulldozer) began to be used to compact the outer portions of the select fill zone, while the central portion was compacted with the hand roller. The front loader operated well onto the select zone at this stage. Finally, when fill covered the crown to a depth of approximately 1.5 ft, the bulldozer began to make compaction passes transversely across the crown of the structure while towing the single-drum vibratory roller. During the last 2 to 3 ft of fill placement both the water truck and the scraper also operated up to several feet onto the select fill zone on a random and occasional basis.

These carefully controlled fill placement and compaction procedures, with care being taken to prevent the occurrence of large vehicular loads in close proximity to the flexible culvert structure, represent a case in which the effects of compaction on culvert deformations and stresses will be significantly less than for more "typical" conditions in which procedural controls are less conscientiously enforced.

The degree of compaction achieved has only a minor effect on the magnitude of soil stresses induced by compaction, but it has a significant influence on the stiffness of the backfill (*1, 2*). For this reason it was also necessary to closely monitor the degree of compaction achieved at all points in order to properly model backfill stress-deformation behavior in the finite element analyses performed. On the basis of constant observation of field operations, as well as 26 in situ density tests, it was judged that compaction control was excellent and resulted in uniformly compacted backfill in both the select fill and the sandy clay fill zones. The average density achieved was approximately 96 percent of the standard Proctor maximum dry density in the select fill zone and 97 percent (at an average water content of 12 percent) in the sandy clay zone. Density variations within each zone were judged to be small.

CONVENTIONAL FINITE ELEMENT ANALYSES

Two types of finite element analyses were performed to evaluate the significance of compaction effects on culvert deformations and stresses: (*a*) conventional analyses without any capacity for consideration of compaction-induced stresses and (*b*) analyses that incorporate recently developed finite element models and algorithms that allow consideration of compaction-induced soil stresses and associated deformations.

Both types of analysis used the hyperbolic formulation proposed by Duncan et al. (*3*) as modified by Seed and Duncan (*1*) to model

nonlinear stress-strain and volumetric strain behavior of the soils involved, varying the values of Young's modulus and bulk modulus in each soil element as a function of the stress state within that element at any given stage of the analysis.

The conventional analyses, without compaction effects, consisted of modeling placement of fill in successive layers or increments. A two-iteration solution process was used for each increment to establish appropriate soil moduli in each element in order to model nonlinear soil behavior. These analyses were performed using the computer program SSCOMP (*4*), a two-dimensional plane strain finite element code.

Figure 1 (bottom) shows the finite element mesh used for these analyses. Only one-half of the culvert and backfill was modeled because of the symmetric nature of both the backfill operations and the measured deformations. Soil elements were modeled with four-node isoparametric elements and the culvert structure and underlying concrete members were modeled with piecewise-linear beam elements. Nodal points at the right and left boundaries of the mesh were free to translate vertically but were rigidly fixed against rotation or lateral translation, which provided full moment transfer at the culvert crown and the centerline of the concrete base slab.

The program SSCOMP models all structural elements as deforming in linear elastic fashion. Table 2 gives the properties used to model the various components of the culvert structure. The concrete footings and base slab were interconnected by reinforcing steel and were modeled as a continuous section. Elastic section moduli for the corrugated aluminum structural plate culvert sections represent values 20 percent less than the theoretical values calculated for these sections. This 20 percent reduction is based on large-scale flexural test data and provides a reasonably accurate model of stress-deformation behavior for 9- x 2 1/2-in. aluminum plate of 0.175-in. thickness at stress levels representing a factor of safety greater than 2.0 with respect to plastic failure in flexure.

TABLE 2 STRUCTURAL PROPERTIES MODELED

Structural Component	E (kip/ft^2)	Area (ft^2/ft)	I (x 10^{-4}) (ft^4/ft)
Concrete walls and invert	464,000	0.75	352.0
Culvert haunch (no ribs)	1,468,800	0.017	0.676
Culvert crown (with ribs)	1,468,800	0.033	4.74
Culvert crown "hinges"	1,468,800	0.033	2.37

Section moduli of the ribbed crown section were modeled as intermediate between the theoretical value for the crown plate and ribs functioning as a composite beam and the theoretical value for the ribs and crown plate each functioning independently. This is again based on large-scale flexural test data and represents the effects of shear slippage at the plate-rib connection. Every alternate crown rib was spliced at one of two locations, and each of these splice locations was modeled as a partial "hinge" of reduced flexural stiffness with a length of 0.1 ft as indicated in Figure 1 (bottom) and Table 2.

Table 3 gives the hyperbolic soil model parameters used to model the select and native backfill zones as well as the existing foundation soils. These parameters were based on triaxial tests of these soils. A series of isotropically consolidated, drained triaxial tests with volume change measurements was performed on the crushed basalt select fill. Samples were compacted to approximately 96 percent of the standard Proctor maximum dry density, taken as representative of field conditions, and were tested at effective confining stresses of between 6.4 and 20.2 psi. Figure 6 shows the results of these tests, as well as the modeled soil behavior based on the soil parameters listed in Table 3. Modeled stress-strain behavior is in excellent agreement with the test results. Modeled volumetric strain behavior agrees well with the test data at low stress levels but provides poor modeling at high stress levels because the hyperbolic soil model cannot model dilatency. An additional pair of triaxial tests was performed to provide a basis for evaluation of unloading-reloading behavior, as shown in Figure 7.

A second series of unconsolidated, undrained triaxial tests was performed to evaluate the behavior of the native backfill. Samples were compacted to approximately 97 percent of the standard Proctor maximum dry density at a water content of 12 percent, again representative of field conditions, and were tested under undrained conditions at confining stresses of between 5.0 and 16.9 psi. Figure 8 shows the results of these tests as well as the modeled soil behavior based on the parameters listed in Table 3. In the absence of volume change data, the two bulk modulus parameters K_b and m were estimated from typical values for similar soils. Two additional tests were performed to evaluate unloading-reloading behavior as shown in Figure 9. The soil model parameters generated for the native backfill zone were also considered suitable for representation of the existing native foundation soil, which was partly desiccated with an in situ water content of approximately 6 to 10 percent.

Figure 10 shows the results of incrementally modeling fill placement without compaction-induced stresses using the program SSCOMP. As shown in this figure, calculated culvert displacements at the crown point are only approximately one-third of the measured values at all fill stages, and the maximum calculated radial deflection of the quarter point is only one-quarter of that measured in the field. It is unlikely that this magnitude of discrepancy between deformations calculated without consideration of compaction effect and the actual field measurements is due to poor modeling of soil or structural stiffnesses, because these are all based on reliable test data, and it thus appears likely that compaction-induced earth pressures significantly influenced the measured field deformations, even though compaction operations were carefully controlled to minimize this influence.

TABLE 3 HYPERBOLIC SOIL MODEL PARAMETERS

Soil Type	γ (kip/ft3)	c (kip/ft2)	ϕ (degrees)	$\Delta\phi$ (degrees)	K	n	R_f	K_b	m	K_{ur}	K_o
Select backfill	0.138	0.0	47.0	0.0	580	0.50	0.63	350	−.15	1080	0.27
Native backfill	0.126	0.85	14.5	0.0	260	0.26	0.81	175	0.30	505	0.70
Native foundation	0.126	0.85	14.5	0.0	260	0.26	0.81	175	0.30	505	0.70

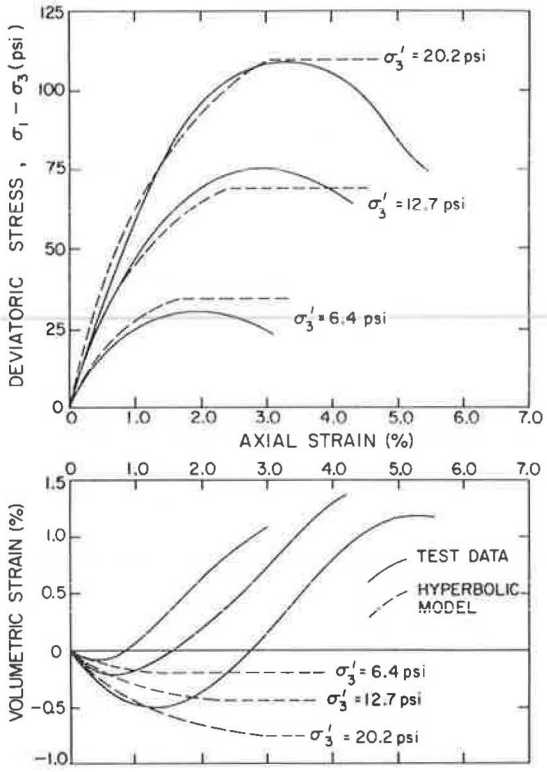

FIGURE 6 Modeled nonlinear stress-strain and volumetric strain behavior of the select backfill versus triaxial test results.

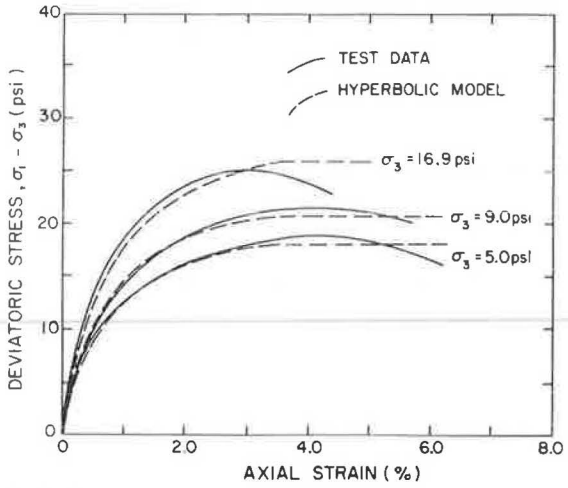

FIGURE 8 Modeled nonlinear stress-strain behavior of the native sandy clay versus triaxial test results.

FINITE ELEMENT ANALYSES WITH COMPACTION EFFECTS

A second set of finite element analyses was performed, again using the program SSCOMP, to model the effects of compaction-induced earth pressures. These analyses again incrementally modeled the placement of backfill in layers, but after each backfill placement increment an additional two-iteration solution increment was used to model the effects of compaction operations at the surface of the new backfill layer. The models and analytical procedures used to simulate compaction effects are described in detail by Seed and Duncan (*1, 2*). Because these are rather complex, only a brief general description follows.

Two soil behavior models are employed in these analyses. Nonlinear stress-strain and volumetric strain behavior are again modeled with the hyperbolic formulation used for the conventional analyses without compaction. The second soil behavior model is a model for stresses generated by hysteretic loading and unloading of soil. This hysteretic model performs two roles during the analyses: (*a*) it provides a basis for the controlled introduction of compaction-induced soil stresses at the beginning of each compaction increment and (*b*) it acts as a "filter" controlling and modifying the compaction-induced fraction of soil stresses during all stages of analysis.

Horizontal stresses within a given soil element are considered to consist of two types or fractions defined as (*a*) geostatic lateral stresses ($\sigma_{x,o}$), which include all stresses arising because of increased overburden loads and deformations that result in lateral stress increases, and (*b*) compaction-induced lateral stresses ($\sigma_{x,c}$), which are the additional lateral stresses arising at the beginning of each compaction increment as a result of transient compaction

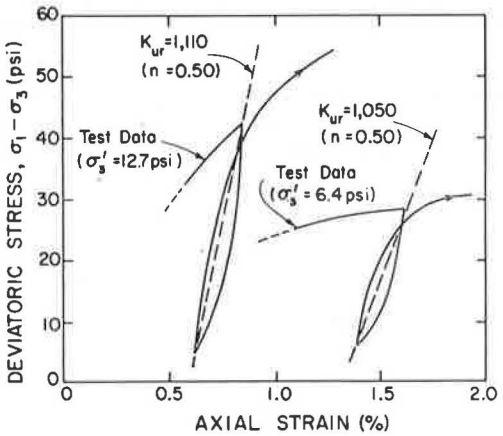

FIGURE 7 Select backfill unloading-reloading stress-strain behavior.

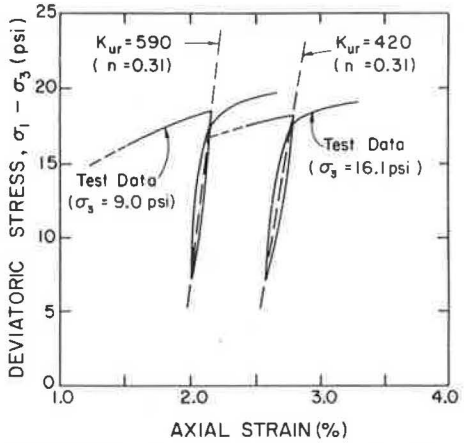

FIGURE 9 Native sandy clay unloading-reloading stress-strain behavior.

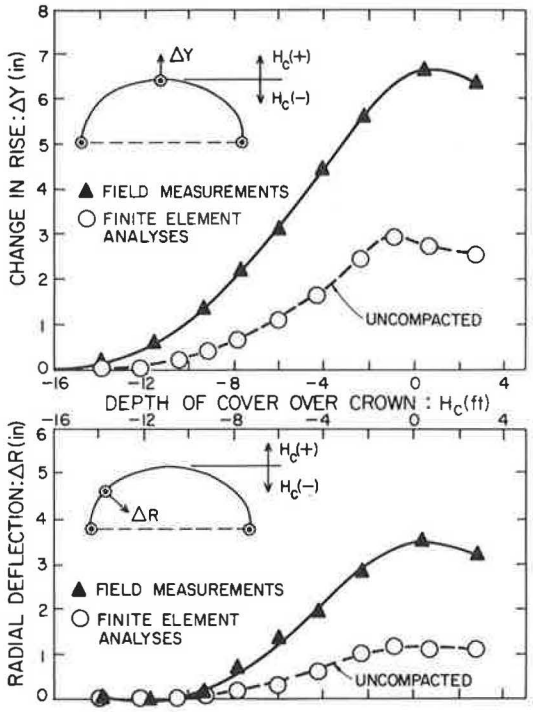

FIGURE 10 Field measurements versus culvert deformations calculated by finite element analyses without modeling compaction effects.

loading. The overall lateral soil stress (σ_x) at any point is then the sum of the geostatic and compaction-induced stresses.

Compaction-induced lateral stresses are introduced into an analysis during "compaction" increments. Both the peak and the residual compaction-induced lateral stresses at any point are modeled based on the peak, virgin compaction-induced horizontal stress increase ($\Delta\sigma_{x,vc,p}$), which is defined as the maximum (temporary) increase in horizontal stress that would occur at any given point as a result of the most critical positioning of any surficial compaction plant loading actually occurring if the soil mass was previously uncompacted (virgin soil). This use of $\Delta\sigma_{x,vc,p}$ allows consideration of compaction vehicle loading as a set of transient surficial loads of finite lateral extent that pass one or more times over specified portions of the fill surface, properly modeling the three-dimensional nature of this transient concentrated surface loading within the framework of the two-dimensional analyses performed. The need to model the most critical positioning actually achieved by each compaction vehicle relative to each soil element at each backfill stage necessitated the constant monitoring of vehicle movements during backfill operations.

$\Delta\sigma_{x,vc,p}$, which is independent of previous hysteretic stress history effects, can be evaluated using three-dimensional linear elastic analyses (*1*) and is directly input for each soil element at the beginning of each compaction increment. The hysteretic soil behavior model then accounts for previous hysteretic loading-unloading cycles (e.g., previous compaction increments) and calculates both the actual peak and residual lateral stress increases on planes of all orientations within a soil element (residual vertical stress remains constant) based on $\Delta\sigma_{x,vc,p}$ and the previous hysteretic stress history of the soil element.

In addition to establishing the magnitude of residual compaction-induced lateral stresses introduced at the beginning of each compaction increment (before nodal displacements and associated stress redistribution), the hysteretic soil behavior model also acts as a "filter" controlling and modifying the compaction-induced component of stress in soil elements at all stages of analysis. All calculated increases in σ_x at any stage during an analysis are considered to represent an increase in geostatic lateral stress and represent hysteretic "reloading" if a compaction-induced stress component is present. Subsequent to the solution of the global stiffness and displacement equations for any increment, therefore, the resulting calculated increases in σ_x are used as a basis for calculating an associated decrease in the compaction-induced fraction of lateral stress ($\sigma_{x,c}$). This progressive erasure or "overwriting" of compaction-induced lateral stresses by increased geostatic lateral stresses results in an overall increase of σ_x less than the calculated increase in $\sigma_{x,o}$ for soil with some previously "locked-in" compaction-induced lateral stress component and corresponds to hysteretic "reloading." When solution of the global stiffness and displacement equations results in a calculated decrease in σ_x, it is assumed that this decrease is borne by both the geostatic and the compaction-induced fractions of the preexisting lateral stress in direct proportion to their contributions to the overall lateral effective stress.

Compaction-induced lateral stress increases in a soil mass can exert increased pressure against adjacent structures, which results in structural deflections that may in turn partly alleviate the increased lateral stresses. Multiple passes of a surficial compaction plant, however, continually reintroduce the lateral stresses relaxed by deflections and result in progressive rearrangement of soil particles at shallow depths. To approximate this process with a single solution increment, both the compaction-induced lateral stresses and the corresponding nodal point forces for a given compaction increment are assumed to represent "following" loading from the current ground surface down to the depth at which $\sigma_{x,c}$ exceeds $\sigma_{x,o}$. All soil elements above this depth are assigned negligible moduli, resulting in calculation of displacements at all locations as a result of compaction-induced lateral forces, but (*a*) no changes in soil stresses result from displacements in soil elements above the specified depth of "following" compaction loading and (*b*) compaction-induced nodal forces in this upper region are also undiminished by deflections.

Four additional soil parameters are needed for the hysteretic model controlling compaction-induced soil stresses, and these may be evaluated by correlation with the soil strength parameters c and ϕ. Seed and Duncan (*1, 2*) provide a detailed description of methods for determining these four parameters, and Table 4 gives the parameters used to model the select fill and native soil zones in the analyses performed. Two parameters $K_{1,\phi,B}$ and c_B define the maximum residual compaction-induced lateral stress that can retained by soil at shallow depth as controlled by potential passive soil failure. The parameter F controls the fraction of peak (transient) lateral stress ($\Delta\sigma_{x,vc,p}$) retained as residual compaction-induced stress. The final parameter (K_3) defines the rate at which geostatic stress increases "overwrite" compaction-induced stresses during hysteretic reloading.

TABLE 4 HYSTERETIC SOIL MODEL PARAMETERS

Soil Type	c_B (kip/ft^2)	$K_{1,\phi,B}$	K_3	F
Select backfill	0.00	4.30	0.11	0.61
Native backfill	0.67	1.11	0.45	0.40
Native foundation	0.67	1.11	0.45	0.40

There is significant scatter in the relationship between F and ϕ for cohesionless soils, and the mean value of F based on correlation with ϕ was used to model the select fill (*1*, 2). There is currently little reliable data on which to base evaluation of F for cohesive soils under short-term conditions, but F in the cohesive native soil zones does not significantly affect stresses and deformations near the Promontory culvert structure, and a value of F = 0.40 was judged to be suitable for modeling the native soil zones in the analyses performed.

Calculation of the peak, virgin compaction-induced lateral stress ($\Delta\sigma_{x,vc,p}$) to be input into each soil element at the beginning of each compaction increment is a time-consuming process. In the "free field" away from the culvert, three-dimensional linear elastic analyses were performed using Boussinesq closed-form solutions to calculate the peak lateral stresses induced at any given depth by each piece of construction equipment. These values were then enveloped to produce a single profile of $\Delta\sigma_{x,vc,p}$ versus depth that was used for all soil elements occurring at a distance of more than a few feet from the culvert at all fill stages.

For soil elements near the culvert it was necessary to carefully review the recorded field observations in order to model peak stresses arising as a result of the most critical positioning (closest proximity) achieved by each piece of compaction equipment at each fill level. At fill levels up to the top of the haunches, the small two-drum vibratory roller controlled peak transient lateral stresses ($\Delta\sigma_{x,vc,p}$) adjacent to the culvert. At fill levels above the hanches, however, larger vehicles began to exert increasing influence on values of $\Delta\sigma_{x,vc,p}$ for soil elements in the region of the quarter point midway between the haunch and crown. If compaction operations had been less carefully controlled and larger vehicles had operated nearer the culvert, the influence of compaction on culvert stresses and deformations would have been greatly increased.

Figure 11 shows the results of incrementally modeling both backfill placement and compaction. Modeling of compaction effects has resulted in significantly improved agreement between calculated and measured culvert deflections at all backfill stages compared with the earlier analyses without compaction. The calculated maximum crown rise (peaking) of 5 in. represents an increase of 80 percent over the maximum peaking of 2.8 in. calculated by conventional analyses without consideration of compaction effects and is only 25 percent less than the value actually measured. Modeling compaction effects also doubled the maximum calculated radial displacement of the quarter point to more than 2 in., and this new value is within 40 percent of the value actually measured.

Whereas the modeling of compaction effects significantly improved agreement between calculated and measured deformations, it must also be noted that peak calculated displacements of the crown and quarter points are still 25 and 40 percent less, respectively, than the values measured in the field. It is likely that this remaining discrepancy is due in large part to the modeling of culvert deformation behavior as linear elastic using the properties listed in Table 2. As was noted previously, this provides fairly accurate modeling of flexural stiffness for the various culvert elements as long as stress levels remain low (representing a factor of safety greater than 2.0 with respect to plastic failure in flexure). Calculated culvert stresses were all well within this range for the earlier analyses performed without modeling compaction effects, but, when compaction was modeled in this second set of analyses,

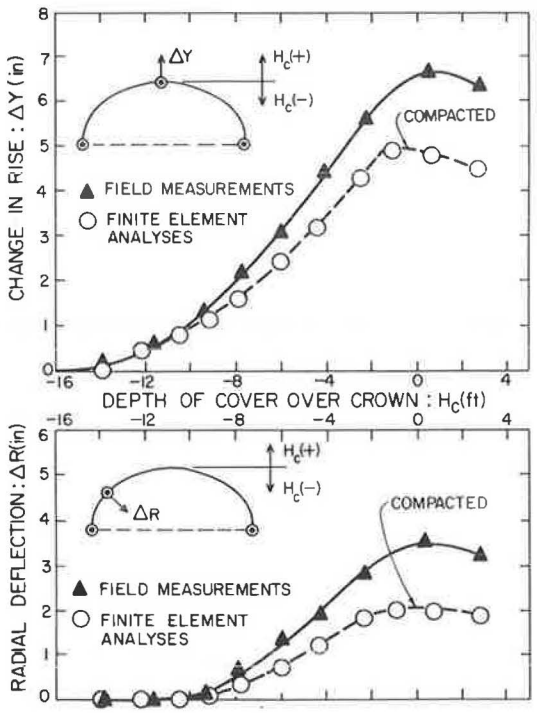

FIGURE 11 Field measurements versus culvert deformations calculated by finite element analyses including modeling of compaction effects.

bending moments calculated in the haunch region were significantly increased to the extent that this linear elastic modeling of culvert behavior greatly overestimated culvert stiffness during the later stages of backfilling.

Figure 12 shows culvert bending moments and axial thrust around the culvert perimeter following completion of backfill operations as calculated in both sets of finite element analyses performed (with and without compaction). In Figure 12*a* it can be seen that modeling compaction effects resulted in increased bending moments in both the crown and the haunch regions. The increased positive crown moment is not of serious concern for design purposes because it is well below the level required for onset of plastic yield (factor of safety = 3.9) and represents an increase in the ability of the crown section to withstand subsequent negative moments that will arise due to live traffic loads. The increased bending moments at the top and base of the unreinforced haunch region are potentially more serious. Without compaction effects the calculated minimum factor of safety with regard to exceeding the plastic moment capacity in the haunch region was 7.4, apparently representing overconservative design. Modeling compaction effects reduced this factor of safety to only 1.4 at the top of the haunch region and 2.0 at the base, and both of these moments correspond to flexure in directions representing potential failure modes.

In Figure 12*b* it can be seen that modeling compaction-induced earth pressures also resulted in calculation of increased thrust around the perimeter of the culvert. This increase, which was between 10 and 25 percent around the culvert perimeter, was much less pronounced than was the effect of modeling compaction on calculated culvert bending moments.

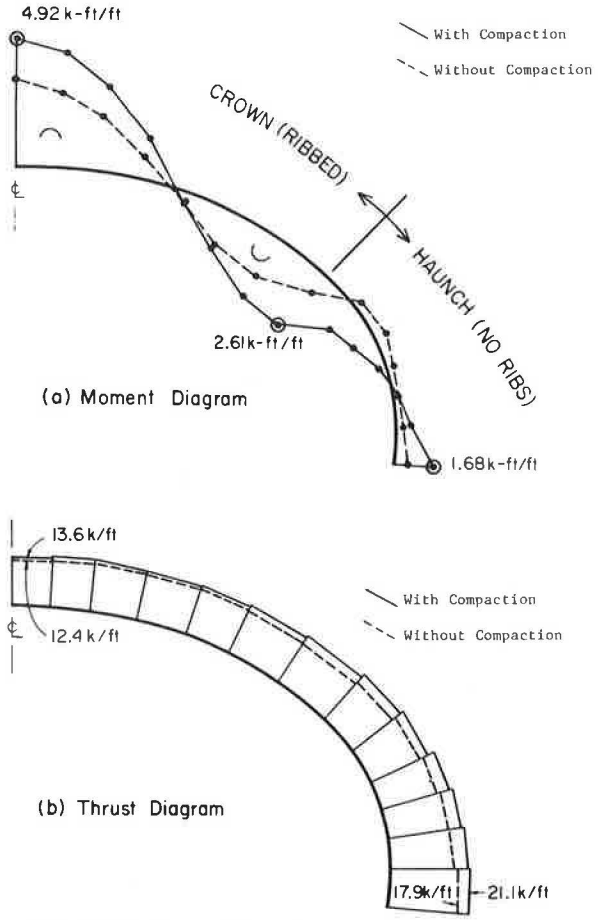

FIGURE 12 Culvert bending moments and perimeter axial thrust calculated by finite element analyses with and without modeling compaction effects.

SUMMARY AND CONCLUSIONS

Incorporation of analytical models and methods for consideration of compaction effects significantly improved the agreement between culvert deformations calculated by finite element analyses and actual field measurements at all stages of backfill placement and compaction. Conventional finite element analyses, which did not model compaction effects, greatly underestimated culvert deformations at all fill stages. Analyses modeling compaction effects produced much better agreement with field measurements, and it was shown that the remaining underestimation of culvert deformations in these analyses may have been due in large part to linear elastic modeling of culvert stress-deformation behavior, which overestimated culvert stiffnesses at the higher culvert stress levels calculated by the analyses that modeled compaction effects.

Calculated culvert stresses were also significantly affected by the modeling of compaction-induced earth pressures. Analyses that included modeling of compaction effects resulted in calculation of higher bending moments at both the culvert crown and the haunch sections, with the increased haunch moments representing the potentially most serious condition. Calculated thrust around the perimeter of the culvert was also increased by inclusion of compaction-induced earth pressures in these analyses, but this effect was less pronounced than the effect of compaction on calculated bending moments.

The results of these analyses, along with the full-scale field measurements, strongly suggest that compaction-induced earth pressures had a significant effect on both the deformations and the final stress state of the Promontory culvert structure. Conventional analyses, without modeling of compaction effects, appear to have resulted in a somewhat unconservative assessment of both culvert stresses and deformations for this case, which involved a very long-span flexible metal culvert structure with relatively shallow final crown cover.

ACKNOWLEDGMENTS

Support for this research was provided by Kaiser Aluminum and Chemical Corporation as well as by the National Science Foundation. This support is gratefully acknowledged. The authors also wish to extend their thanks to Mony Antoun of Kaiser Aluminum and Chemical Corporation for his valuable assistance during the field operations involved in this project.

REFERENCES

1. R. B. Seed and J. M. Duncan. *Soil-Structure Interaction Effects of Compaction-Induced Stresses and Deflections*. Geotechnical Engineering Research Report UCB/GT/83–06. University of California, Berkeley, 1983.
2. R. B. Seed and J. M. Duncan. FE Analyses: Compaction-Induced Stresses and Deformations. *Journal of the Geotechnical Engineering Division*, ASCE, Vol. 112, No. 1, Jan. 1986, pp. 23–43.
3. J. M. Duncan, P. Byrne, K. S. Wong, and P. Mabry. *Strength, Stress-Strain and Bulk Modulus Parameters for Finite Element Analyses of Stresses and Movements in Soil Masses*. Geotechnical Engineering Research Report UCB/GT/80–01. University of California, Berkeley, 1980.
4. R. B. Seed and J. M. Duncan. *SSCOMP: A Finite Element Program for Evaluation of Soil-Structure Interaction and Compaction Effects*. Geotechnical Engineering Research Report UCB/GT/84–02. University of California, Berkeley, 1984.

Publication of this paper sponsored by Committees on Subsurface Soil-Structure Interaction and on Culverts and Hydraulic Structures.